# Current Progress on Power Management Systems for Triboelectric Nanogenerators

Tingshu Hu, *Senior Member, IEEE*, Haifeng Wang, *Member, IEEE*, William Harmon, David Bamgboje, *Member, IEEE*, and Zhong-Lin Wang

***Abstract*—This article presents a review on the development of power management systems (PMSs) for triboelectric nanogenerators (TENGs). The TENG is the most recent technology to harvest ambient mechanical energy from the environment and human activities. Its invention was motivated by the prospect of building self-powered systems. The TENG has several appealing advantages, such as high power density, high voltage output, high efficiency at low frequency, and low cost. However, due to the TENG's unique nonlinear electrical property and capacitive behavior, the development of its PMS has presented great challenges as compared to other energy harvesters. The objective of PMS design has evolved from boosting the peak output power, to increasing the energy stored in a capacitor, and to increasing the steady-state output power of a resistive load by using a power converter. Driven by the need to build self-powered systems, the switches in the TENG PMS have evolved from active switches to passive switches. The past decade has witnessed exciting breakthroughs in the development of TENG PMS, yet there are still unlimited opportunities in exploring TENG's energy generation mechanism and vast potential in boosting energy extraction from the TENG by designing effective power converter topologies.**

***Index Terms*—Energy harvesting, power converter, power management, triboelectric nanogenerator (TENG).**

## I. Introduction

THE triboelectric nanogenerator (TENG) is the most recent technology to harvest ambient mechanical energy from the environment and human activities. It was invented in 2012 by Wang *et al.* [1], [2], following the invention of the piezoelectric nanogenerator (PENG) in 2006 [3]. The development of both the PENG and TENG was motivated by the prospect of building self-powered systems—a system that is self-sufficient in energy, which is harvested from its working environment [4]–[6]. Fig. 1 illustrates a self-powered system using energy harvested from TENGs to power electronic devices.

The self-powered or human-powered systems have been a naturally appealing concept [7]–[9], for example, to charge a cellphone using the mechanical energy from walking [10], and have been explored by researchers before the advent of the nanogenerators. The feasibility of human-powered wearable computing was explored in [8], [9] with a detailed analysis of power generation through daily activities. Kymissis *et al.* [7] presented three devices built inside shoes to harvest energy with three different energy harvesting mechanisms, using a magnetic generator and piezoelectric materials. A backpack was developed in [11] to harvest energy while walking with loads.

Recent years have witnessed an upsurge of research efforts in energy harvesting for self-powered and human-powered systems, which are propelled by the increasing needs for portable, wearable electronics and sensors, in Internet of Things and artificial intelligence [8], [12]–[20]. Almost all these electronic devices and sensors are powered by batteries, which have limited life span and need frequent replacement or recharging, posing inconvenience, and challenges in many applications [5], [8], [13], [15], [16], [21], [22]. Furthermore, the disposal of trillions of used batteries will present severe environmental issues. However, if the energy in the environment and human body can be harvested and used to power these electronic devices and sensors, it will provide a clean and sustainable solution to reduce or eliminate the impediment of batteries while avoiding a potential environmental crisis [8], [15], [23].

A conventional approach to harvest biomechanical energy is based on electromagnetic generators, which was adopted in [11], [24]–[27] to harvest energy from walking. The piezoelectric effect enabled the development of more compact and lighter weight generators. In [28], the energy expended during respiration by the relative motion of the ribs was harvested and used to power implanted devices by using PVDF films. In [13], a hybrid piezoelectric/permanent magnet energy scavenging topology was proposed to harvest energy from human walking. A revolutionary development was made in [3], where the piezoelectric effect was explored at the nanoscale, with the invention of a PENG based on zinc oxide nanowire array. This nanogenerator has a potential to harvest almost all forms of mechanical energy and has generated a substantial amount of interest in research communities, with efforts devoted to searching for more advanced materials, enhancing its designs, and widening its applications [29], [30].

The TENGs came as the most recent breakthrough to harvest mechanical energy. According to Wang in [4], the TENG

Manuscript received September 14, 2021; revised January 5, 2022; accepted February 19, 2022. Date of publication March 7, 2022; date of current version April 28, 2022. Recommended for publication by Associate Editor G-S. Seo. *(Corresponding author: Tingshu Hu.)*

Tingshu Hu is with the University of Massachusetts Lowell, Lowell, MA 01854 USA (e-mail: tingshu_hu@uml.edu).

Haifeng Wang is with the Penn State New Kensington, New Kensington, PA 15086 USA (e-mail: hzw87@psu.edu).

William Harmon is with the Raytheon Technologies, Waltham, MA 02451 USA (e-mail: wch7693@gmail.com).

David Bamgboje is with the ePROPELLED, Lowell, MA 01852 USA (e-mail: dbamgbs@gmail.com).

Zhong-Lin Wang is with the Beijing Institute of Nanoenergy and Nanosystems, Chinese Academy of Sciences and Georgia Institute of Technology, Atlanta, GA 30332 USA (e-mail: zhong.wang@mse.gatech.edu).

Color versions of one or more figures in this article are available at https://doi.org/10.1109/TPEL.2022.3156871.

Digital Object Identifier 10.1109/TPEL.2022.3156871

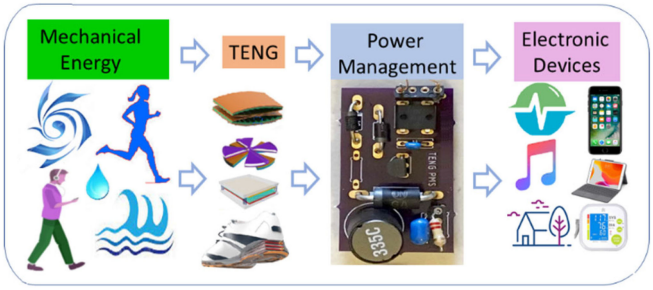


Fig. 1. Illustration of a self-powered system using energy harvested with TENGs. A PMS is needed to convert the TENG's output into a regulated form suitable for electronic devices.

can be applied to harvest all kinds of mechanical energy that is available in our daily life, such as human motion, walking, vibration, mechanical triggering, rotational energy, wind, automobile motion, flowing water, rainfall, tides, and ocean waves [31]–[39]. As compared with other nanogenerators and electromagnetic generators, TENGs have many advantages and unique qualities, including high power density, high voltage output, high efficiency at low frequency, low cost, light weight, robustness, high reliability, and flexible choices for materials [16], [29], [40]–[42]. A very appealing advantage of the TENG is environmental friendliness due to the use of low-cost organic materials, lower manufacturing cost, and lower $CO_2$ emissions as compared with other types of energy harvesting technologies, such as PV technologies [43]. The TENGs are also called organic nanogenerators since the most useful materials are organic and can be very cheap and easy to manufacture, like papers, fabrics, polyester, and PTFE [4]. In [44], a recyclable and green TENG that can fully dissolve and degrade into environmentally benign end products is developed.

Nevertheless, with so many desirable advantages, TENGs appear to be the most difficult to be used directly due to the high voltage pulsed output and the high internal capacitive impedance. In fact, almost all electrical energies harvested with nanogenerators have their shortcomings. A power management system (PMS) must be used to convert the harvested raw energy to a well-regulated form, which is suitable for electronic devices. The invention of the PENG in 2006 was followed by the development of its PMS in 2009–2011 [45]–[49] and presently there are commercially produced PMS for PENG available. Since the invention of TENG in 2012, tremendous efforts have been devoted to the development of its PMS via various routes, with some exciting breakthroughs as reviewed in [50]. More recently, a fully functional self-powered PMS for TENG was developed in [51]. However, due to the TENG's unique nonlinear electrical properties and the capacitive behavior, the energy that can be extracted from the TENG depends on its interaction with the external circuit, and the maximum energy that can be extracted from the TENG by any circuit remains unknown. There is still a vast potential to substantially increase the energy generation of the TENG and the output power of the PMS by searching for the most effective circuit topologies.

This article gives a review of the existing PMSs for TENGs. The first attempt to improve the output of a TENG by using an external circuit can be dated back to 2013 [52], where an instantaneous discharging mechanical switch is designed to short circuit the TENG during certain operation, in order to increase the peak output power. During the past few years, the objectives of power management have evolved from increasing the peak output power to boosting the transferred charges, to increasing the energy stored in a capacitor, with the latest efforts focused on increasing the steady-state output power of a resistive load via a power converter, such as a buck converter and a flyback converter. Earlier works used MOSFETs and logic circuits for the power converters. Realizing that the MOSFETs and logic circuits need an additional power supply, which defeats the purpose of self-powered systems, the most recent efforts turned to using passive switches, such as an SCR in [51] and a spark switch in [53]. These recent results present strong proof of concept for self-powered systems with the TENG as the energy harvesting unit. They also demonstrate the critical and indispensable role of power electronics in the power management of nanogenerators for self-powered systems. However, it should be mentioned that none of these recent results have been published in a journal in electrical engineering.

The purpose of this review is to introduce the problem of power management of nanogenerators to the electrical engineering community, in hopes of attracting the attention of more experts on power electronics to this meaningful, exciting, and promising research area. TENGs are perhaps the most fascinating energy harvesters, not only due to the energy generation mechanism of electrification and electrostatic induction, but also the unique electrical property with nonlinear time-varying internal capacitance. After ten years of research and many publications, it is still not clear what is the optimal strategy to extract the most energy from a TENG. Various circuit topologies have been proposed for the design of switched power flow paths, including, short circuiting the TENG when the internal capacitance is maximum or minimum, changing the connection of external capacitors between series and parallel connections, using different rectifiers such as halfwave, full wave and Bennet's doubler and using different power converters such as buck converter and flyback converter. In our recent paper [54], it was reported that the same PMS and TENG system produced two different steady states, with the output power of one steady state 30% higher than the other, and the reason behind the difference is the TENG's nonlinear internal capacitance. The nonlinear and time-varying electrical property of the TENG seems to provide endless opportunities and a fascinating research platform, for power electronics engineers, to design circuit topologies to improve TENG's energy generation. Other design challenges, such as energy storage, output regulation, and power management of hybrid generators will also be discussed in this review.

## II. TENG's Energy Harvesting Mechanism and Electrical Model

The triboelectric effect is an everyday experience. It is a type of contact electrification that happens when two surfaces of different materials come into contact and then separate. The resulting electrostatic charges are generally a nuisance but may cause real damages to sensitive electronics and be hazardous in the workplace and nature, such as causing a wildfire [4]. This

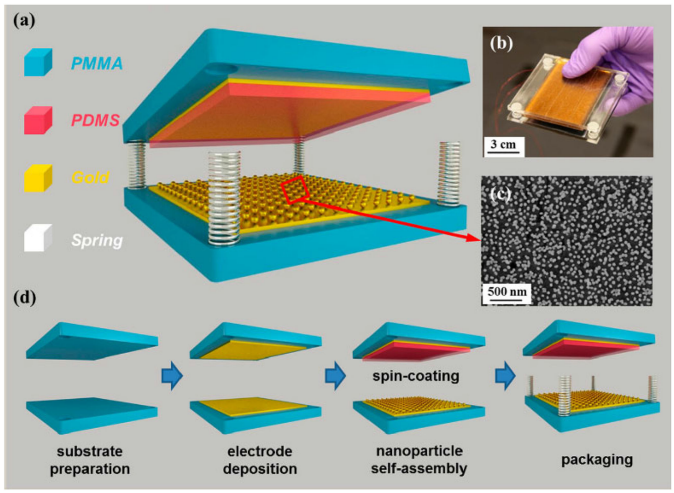


Fig. 2. (a) Schematic of a TENG and (b) photograph of a fabricated TENG. (c) SEM image of gold nanoparticles coated on gold surface. (d) Process flow for fabricating the TENG [55].

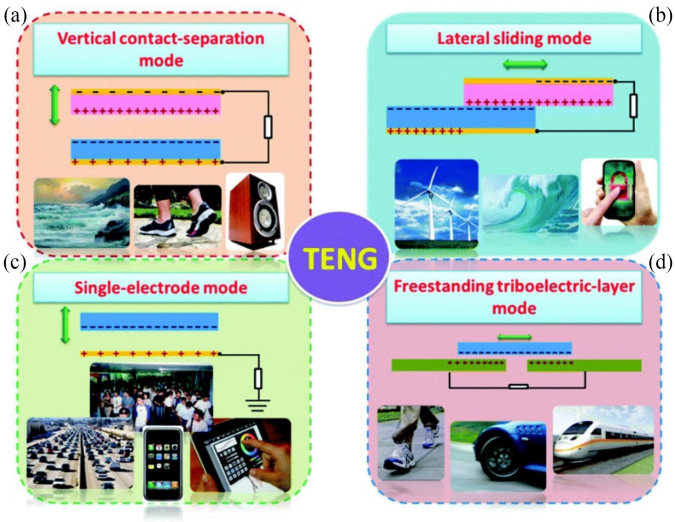


Fig. 3. Four modes of TENG operation [5].

same triboelectric effect was exploited for the first time to build a generator in [1] and [2], later called TENG, to convert the otherwise wasted mechanical energy into a useful resource for mankind. As such, the construction of a TENG is very simple and straightforward—with two surfaces of different materials, each attached to an electrode. The two surfaces are placed in such a way that a certain mechanical motion will drive them into contact and then separate them. Fig. 2 shows the construction of a TENG, a photograph of a fabricated TENG, and the process for fabricating a TENG [55].

When the TENG is pressed with fingers, the two surfaces come into contact. When the pressing force is removed, the four springs at the corners will drive the two surfaces apart. A TENG device with similar construction (but with flexible materials) can be placed inside the shoe to harvest biomechanical energy while walking. Since the first TENG was reported in [1] and [2], four different types of TENGs have been developed based on four fundamental working modes (see Fig. 3 as duplicated from [5]), to harvest energy from different mechanical motions: vertical contact separation mode [1], [2], [55], [56] [as pictured in Figs. 2 and 3(a)], in-plane sliding mode [55] [see Fig. 3(b)], single electrode mode [57] [see Fig. 3(c)], and free-standing mode [58] [see Fig. 3(d)]. With these four modes of TENGs, all kinds of mechanical energy can be harvested [4], [5], ranging from finger typing, engine vibration, walking (mode 1, mode 3), to wind energy, hydropower (mode 2), and raindrop, airflow, and rotating tire (mode 3, mode 4). These four types of TENGs have also been used to construct numerous active sensors, for example, pressure sensors, acoustic sensors, body motion sensors, vibration sensors, and biosensors [5]. Later research efforts have been devoted to the optimization of structural and material designs to enhance the output power, the energy conversion efficiency, device robustness and to widen the applications of the TENGs [59]–[63].

As mentioned in the introduction, to convert the raw energy harvested by TENGs into regulated and steady power that is suitable for electronic devices, a PMS is indispensable. To build a PMS for a TENG, it is fundamental to understand its electrical properties.

A TENG generates electricity due to the coupling of contact electrification and electrostatic induction. Contact electrification provides static polarized charges and electrostatic induction is the main mechanism that converts mechanical energy to electricity. Although contact electrification has been documented for 2600 years, the scientific understanding of the mechanism remains debatable and inconclusive [64]–[67], thus there is no universal model for the description of charge generation from contact electrification. However, for a particular material, its triboelectric property can be quantitatively measured with a parameter, the triboelectric charge density, denoted as $\sigma$. In [67], a standard experimental method was developed to quantify the charge density of a series of materials. The charge density is the main parameter to determine the amount of charge generated due to contact electrification. Since the invention of the TENG, continuous efforts have been devoted to increasing the triboelectric charge density by modifying material composition, improving effective contact area, and changing environmental conditions [68], [69].

For a contact and separation mode TENG, denote the short circuit charge due to contact electrification as $Q_{\rm sc}$, the area of the electrodes as $S$, the distance between the triboelectric layers as $x$, then by [70]

$$Q_{\rm sc} = \frac{S\sigma x\left(t\right)}{d_0 + x\left(t\right)} \tag{1}$$

where $d_0$ is the effective dielectric thickness. The voltage $(V)$ between the two electrodes of a TENG device has two contributions, one from the triboelectric charges, denoted as $V_{oc}(x)$, the other from electrostatic induction due to its capacitive property (without the triboelectric charge, the device is basically a capacitor). By the superposition principle, $V$ can be expressed as the sum of two terms [71]

$$V = -\frac{Q}{C_{\rm Teng}\left(x\right)} + V_{oc}\left(x\right) \tag{2}$$

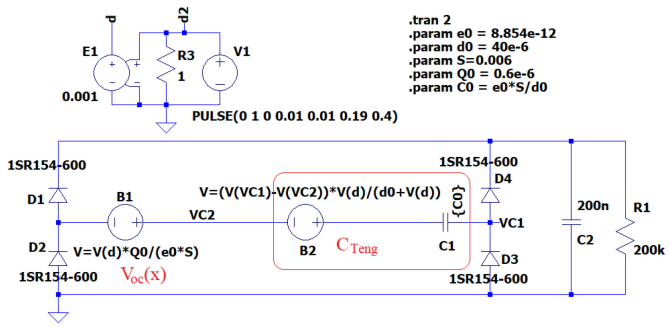


Fig. 4. LTspice model for a TENG with a full-bridge rectifier.

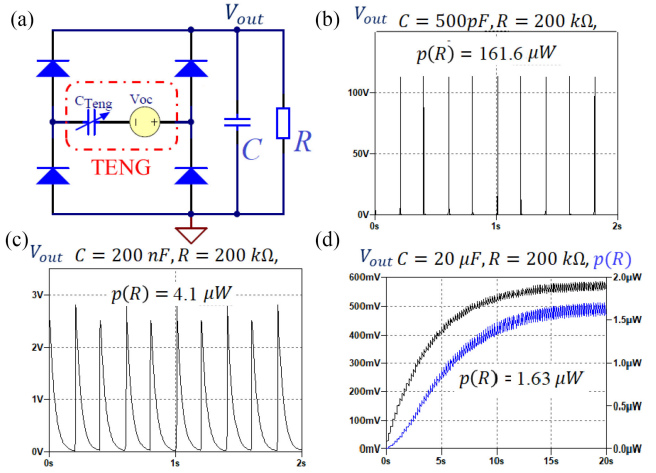


Fig. 5. (a) Circuit model of TENG with a full-wave rectifier and a capacitive filter. (b)–(d) Output voltage and power under three values of filter capacitance: 500 pF (b), 200 nF (c), 20 $\mu$F (d).

where $Q$ is the transferred charges, and $C_{\text{Teng}}(x)$ is the capacitance between the two electrodes, which is given by

$$C_{\text{Teng}}\ (x) = \frac{S\varepsilon_0}{d_0 + x} \tag{3}$$

where $\varepsilon_0$ is the permittivity of free space. Under short circuit condition, $V = 0$, it follows from (1)–(3) that

$$V_{oc}\ (x) = \frac{Q_{\text{sc}}}{C_{\text{Teng}}\ (x)} = \frac{\sigma x}{\varepsilon_0}. \tag{4}$$

From (2), it is clear that a TENG can be modeled as an open-circuit voltage source in series with a time-varying capacitor, as illustrated in Fig. 5(a), inside the red dashed box. The capacitance $C_{\text{Teng}}$ takes the maximum (minimum) value when the two triboelectric surfaces are in contact (at maximum separation). This property has been utilized for the design of switching strategies for a PMS. Circuit models for other TENG modes can be found in [4], [70], [71], [74], and [75].

As the TENG is pressed and released, the separation distance $x$ becomes a function of time, which in turn determines $C_{\text{Teng}}(x)$, $V_{oc}(x)$ in (3) and (4). These nonlinear functions make it nearly impossible to derive analytical solutions for a TENG system, except for very special cases, e.g., when the load is a resistor or a capacitor [71]. A general method that works for all TENG systems is to utilize SPICE software [71], [76]. In [51], [54], and [77], LTspice is used for simulation.

More recently in [78], a simple and stable LTspice model for TENG is developed based on the Miller Theorem, by equivalently representing $C_{\text{Teng}}(x)$ as the series connection of an arbitrary behavioral voltage source B2 and a constant capacitor C1, see Fig. 4, which shows an LTspice model for a TENG connected to a full bridge rectifier (The LTspice model can be downloaded via [79], together with another simulation model for a PMS). The voltage source B1 represents $V_{oc}(x)$; B2 and C1 together realize the nonlinear $C_{\text{Teng}}(x)$ by Miller Theorem. All the parameters for the TENG are given in the list at the top-right and can be easily changed for a particular TENG. Note that the charge density $\sigma = Q0/S$. The voltage at node d, denoted as V(d), represents the distance function $x$, which is generated by the voltage source V1. It can be set up as a pulse function, a sinusoidal function, or an arbitrary piecewise linear (PWL) function provided as a plain txt file (an example can be found via [79]), which can be obtained from the measurement of the real displacement of a TENG device over a number of cycles. In the model in Fig. 4, V1 is a pulse function with period 0.4 s, rise-time/fall-time 0.01s, staying at max value 1 (and min value 0) for 0.19 s. The parameter 0.001 for E1 scales the pulse function such that $x =$ V(d) varies between 0 and 0.001 m.

For a general ac energy harvester, such as a PENG, a full bridge rectifier with a lowpass filter would produce an acceptable output voltage (e.g., see [45]). However, such a simple treatment is not effective for TENGs, due to the internal capacitance $C_{\text{Teng}}$. As the TENG is pressed and released periodically, both $V_{oc}(x)$ and $C_{\text{Teng}}(x)$vary periodically. To demonstrate the effect of $C_{\text{Teng}}(x)$, simulation was conducted on the LTspice model in Fig. 4, with R1 = 200 k$\Omega$ and C2 taking three different values of 500 pF, 200 nF, 20 $\mu$F, respectively. The output voltage and average power on R1 for the 3 values of C2, are shown in Fig. 5(b)–(d).

The output voltage produced with a small capacitance 500 pF is sharply pulsed with a peak voltage of greater than 100 V and very short duration. As the capacitance is increased, the duration of the pulses is increased, and the peak-to-peak ripple size is reduced. However, the average power on the resistor reduces from 161.6 $\mu$W (with 500 pF) to only about 1.63 $\mu$W (with 20 $\mu$F). The result clearly demonstrates that the traditional approach cannot yield the maximal output power and well-regulated output at the same time.

## III. Earlier Development of PMSs and Energy Storage

The objectives of power management for TENGs have evolved from enhancement of instantaneous output power, enhancement of current, to energy storage in capacitors/batteries, and to enhancement of steady output power at low voltage levels which are compatible with most electronics in applications. This section will review the earlier development of PMS for boosting the instantaneous output power, delivering the output energy to a resistive load, and storing the energy in a capacitor. The subsequent sections will be dedicated to the development of PMS for boosting steady output power at low voltage levels, by using various power converter topologies and switching strategies.

The first efforts to manage the power of TENGs can be dated back to 2013 [52], where a mechanical switch is built together

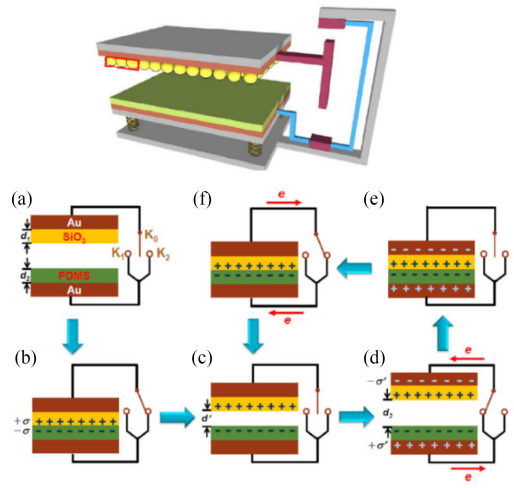


Fig. 6. TENG with a mechanical switch and the operation of the switch [52].

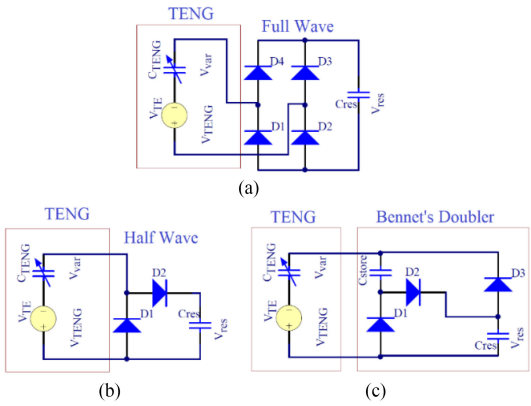


Fig. 7. Three rectifying topologies for storing energy in a capacitor.

with the TENG device (see Fig. 6). This switch short circuits the TENG when the two surfaces are in contact ($C_{\text{Teng}} = \max$) or at maximum separation ($C_{\text{Teng}} = \min$). This simple mechanism can significantly increase the instantaneous peak output power of the TENG by up to 1000 times, while maintaining the same output energy. In [80], a unidirectional mechanic switch is developed for a sliding mode TENG, and in [81], an electrostatic vibration switch in series with the TENG is developed, with similar functions.

Since the mechanical switch may complicate the structural design, an electrostatic vibrator switch and an air-discharge switch were developed in [82] and [83], to implement the same function of the mechanical switch. Switches of similar mechanisms were explored later in [84] and [85] for maximizing the energy that can be delivered to a resistor in one cycle.

The next stage of PMS development is driven by the need to provide steady and stable power to electronics. A TENG's direct output, for a resistive load, is alternating and contains high voltage pulses, which are not suitable for most consumer electronics. A simple solution is to store the pulsed energy in a capacitor or a battery [86], [87]. Fig. 7 depicts three rectifying topologies for storing the energy in a capacitor $C_{\text{res}}$, where Fig. 7(a) is based on a full wave rectifier, Fig. 7(b) a half wave rectifier and Fig. 7(c) Bennet's doubler.

Generally, there is a maximum saturation voltage for the storage capacitor $C_{\text{res}}$. Research efforts have been devoted to increasing the saturation voltage level. In [88], the full-wave rectifier topology was investigated. To increase the saturation level, a switch in parallel with the TENG is used to short circuit the TENG when $C_{\text{Teng}}$ is at its maximum or minimum, with the same operation mechanism as the one presented in Fig. 6 [52]. It is reported that the saturation level of $V_{\text{res}}$ can be doubled as compared to what can be achieved with the topology in Fig. 7(a).

An interesting and somewhat surprising result in this direction is reported in [77] and [89], where Bennet's doubler is utilized as a rectifier for energy storage [see Fig. 7(c)]. Bennet's doubler was later adopted for the development of an inductor free output multiplier in [90] and a programmed TENG in [91]. This topology requires no switch, since the diodes automatically turn the two capacitors from series connection (when charged by the TENG) to parallel connection (when discharging), and vice versa. During the initial charging cycles, the increase of the energy stored in $C_{\text{res}}$ in Fig. 7(c) is much slower than the other two topologies in Fig. 7(a), (b). After many cycles, say 300, the energy stored in $C_{\text{res}}$ will exceed the maximum saturation level achieved by the other two topologies and continues to grow, exponentially, only to be limited by the breakdown voltage of the diodes and the capacitors. The reason behind this exponential growth is the nonlinear and time-varying capacitance of the TENG. If $C_{\text{Teng,max}}/C_{\text{Teng,min}} > 2$, the circuit will become unstable, causing the exponential growth. This condition is easily satisfied by most TENGs.

Fig. 8 (from [77]) compares the charging of the capacitor $C_{\text{res}}$ under the 3 topologies for a TENG device with a contact force of 1.33 N, and the TENG is pressed and released at 5 Hz frequency. Other parameters for the TENG device and the 3 circuits can be found in [77].

The comparison in Fig. 8(d) shows the dependence of energy stored per cycle on the voltage across $C_{\text{res}}$, which demonstrates the unique nonlinearity of the TENG's electrical property. For the half-wave and full-wave topology, the energy stored per cycle reaches a peak value then decreases to 0, but for Bennet's doubler, it increases monotonically with $V_{\text{res}}$. Thus theoretically, the energy stored in $C_{\text{res}}$ per cycle is unlimited, or only limited by the voltage rating of the circuit elements, e.g., 800 V, as depicted in Fig. 8(d). In this regard, the maximum energy that can be extracted from a TENG device is unknown, or need to be well defined, by taking into account technical issues from implementation. To show the effectiveness of the strategy with Bennet's doubler, the capacitance of $C_{\text{res}}$ used in [77] is a few nF and the voltage $V_{\text{res}}$ needs to be a few hundred volts, which is too high for typical small electronics. Another issue with this charging topology is that it takes hundreds of cycles to show the advantage over other topologies, which may be too slow if there is an immediate requirement for the energy. These issues need to be addressed with more advanced circuit topologies based on power converters, which will be discussed in subsequent sections.

## IV. Switched Capacitors With Mechanical Switch

Switching the capacitors from series connection to parallel connection seems to be a straightforward approach to stepping

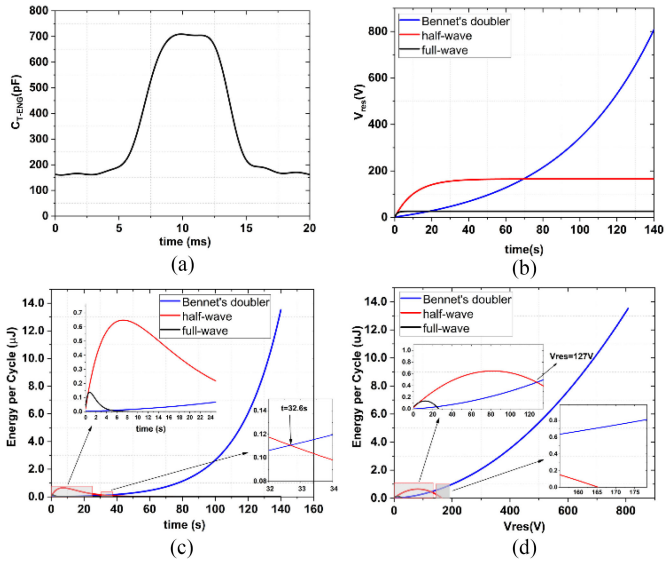


Fig. 8. Experimental comparison of the output characteristics of the half and full-wave rectifiers with Bennet's doubler for the $10 \times 10$ $\mathbf{cm}^2$ device with contact force of 1.33 N. (a) Variation of $\boldsymbol{C_{\mathrm{Teng}}}$ in one cycle of operation measured by the technique in [77]. (b) Charging curves across $C_{\mathrm{res}}$ for the three conditioning circuits. (c) Stored energy per each cycle in $C_{\mathrm{res}}$ for the three conditioning circuits. (d) Stored energy in $C_{\mathrm{res}}$ as a function of $V_{\mathrm{res}}$.

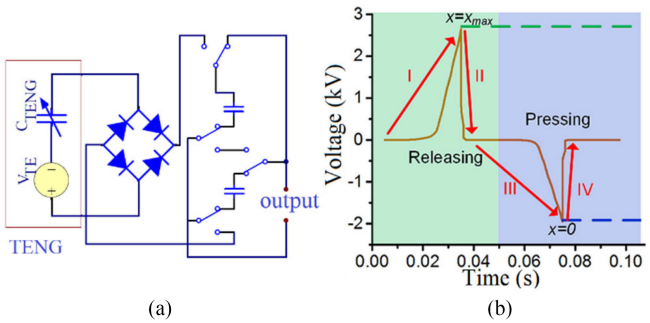


Fig. 9. (a) Stepping down the voltage with switched capacitors [94]. (b) Four phases of a motion cycle [85].

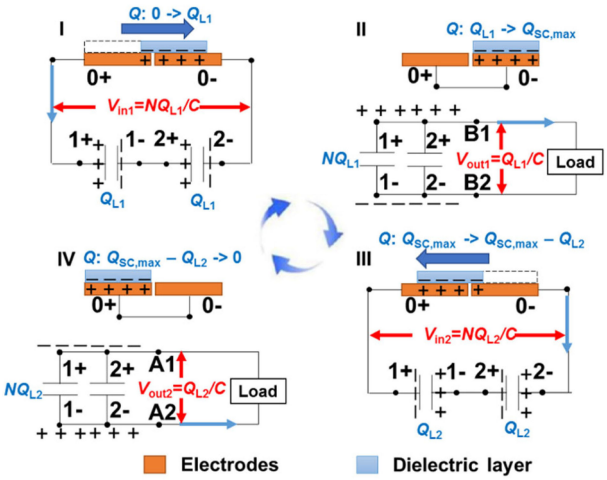


Fig. 10. Switched capacitors for a sliding mode TENG [95].

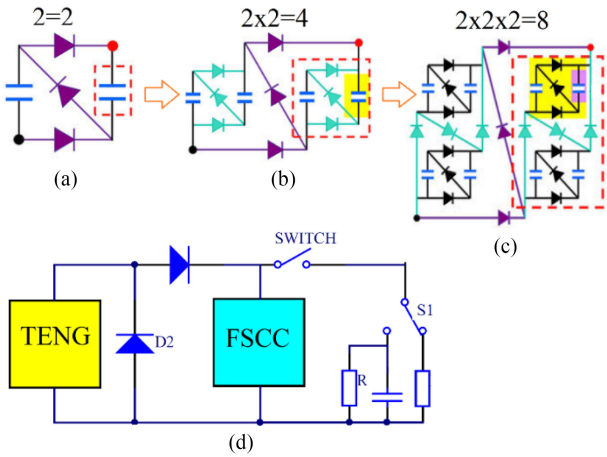


Fig. 11. (a)–(c) Fractal design of switching capacitors. (d) PMS based on fractal switching capacitors [96].

down the voltage. This approach may provide an ideal solution to supplying power to small electronics since there is no need for bulky inductors or transformers [92]. The switched capacitors were used in [93] to construct a steep step-down buck converter to deliver an output voltage of about 1 V. In [94], the switched capacitor strategy is employed to step down the output voltage of a contact and separation mode TENG for the applications in self-powered wireless sensor nodes.

Fig. 9(a) shows a diagram of the PMS in [94] with two switched capacitors. The switching scheme seems to be simple. The capacitors are in series when charged by the TENG and in parallel when discharging to the load. With a full-wave rectifier, the capacitors are charged when the separation distance $x$ increases from 0 to the maximum or decreases from the maximum to 0. Fig. 9(b) illustrates the four phases in a motion cycle.

In phase I, the separation distance $x$ increases from 0 to the maximum, and the capacitors are charged while in a series connection. In phase II, $x$ stays at the maximum, and the capacitors are switched to parallel and discharge immediately. In phase III, $x$ decreases from the maximum to 0, and the capacitors are charged while in series. In phase IV, $x$ stays at 0, the capacitors discharge while in parallel and then get ready for the next motion cycle before $x$ starts to increase.

Due to the simple relationship between the TENG's charging state and the mechanical motion, a mechanical switch can be designed based on the TENG's motion. Note that the change of state for the switches in [94] is the same as the switch in [52]. Experiment is conducted with 2, 4, 8 switching capacitors and varying load resistance. As the number of capacitors is increased, the peak output voltage is reduced from around 60 to 15 V, but the power remains about the same.

In [95], a similar switching capacitor strategy was employed and a motion-triggered mechanical switch is designed for a sliding mode TENG, see Fig. 10, for the change of connection of the capacitors based on the TENG's motion.

The idea of switching capacitors is further explored in [96] with a more intricate design, called a fractal design, to switch the connection of many more capacitors (up to 96 in [96]).

Fig. 11(a)–(c) shows the fractal design of $2^N$, $N = 1, 2, 3$, capacitors, respectively. The topology of $2^{N+1}$ design is obtained by replacing each capacitor in the $2^N$ circuit with a basic

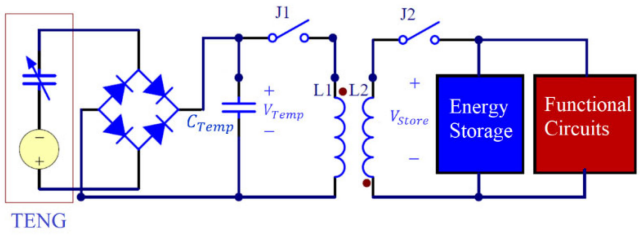


Fig. 12. PMS based on a flyback converter [72].

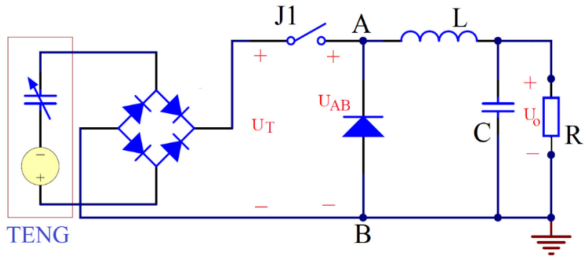


Fig. 13. PMS based on a buck converter.

connection in Fig. 11(a). A noticeable advantage over [95]'s design is that the switching is automatically implemented with the diodes, as with the automatic switch in [77], [92], [93], i.e., the capacitors are in series when charged, and in parallel when discharging. Fig. 11(d) shows the circuit diagram of the PMS in [96], where FSCC represents the fractal network of the capacitors charged by the TENG via a half-wave rectifier. Although the connection of the capacitors inside the FSCC is switched automatically, the main switch on top of the circuit is implemented mechanically based on the TENG's motion. The switch S1 is a manual switch for choosing the type of load.

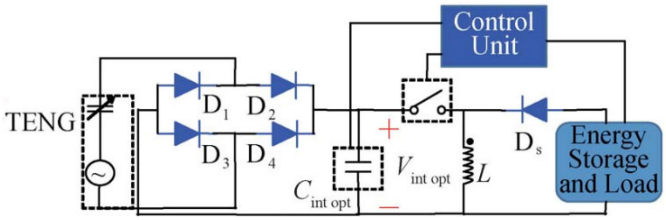


Fig. 14. PMS based on a buck–boost converter [99].

## V. Power Converter Topologies With Active Switches

Further driven by the application needs for supplying low-voltage power to small electronics, research efforts in recent years have been devoted to converting the TENG's high voltage output to a level which is compatible with the power supply voltage of typical portable electronics. The well-established buck converter, flyback converter, and buck-boost converter topologies in power electronics seem to be ready-to-use for this objective.

The first effort along this direction is reported in [72], where a flyback converter is used to step down the voltage across the diode bridge, $V_{\text{Temp}}$ to $V_{\text{Store}}$ (see Fig. 12), which is compatible with functional electronic devices.

The operation of the circuit can be described as follows. Initially, $V_{\text{Temp}} = 0$ and both switches are open. As the TENG is mechanically agitated, it charges $C_{\text{Temp}}$. When $V_{\text{Temp}}$ reaches an optimal value (where impedance match condition is satisfied), the switch J1 is closed and the energy in $C_{\text{Temp}}$is transferred to L1. When $V_{\text{Temp}}$ drops to 0, J1 is open and J2 is closed, causing the energy in L1 to be transferred to L2, then to the energy storage unit, typically a bulk capacitor, and then to the functional circuit. When the current of L2 decreases to 0, J2 opens and prepares for the next cycle. The switches J1 and J2 are implemented with MOSFETs and controlled by a logic circuit. The effectiveness of this PMS has been verified by experiment.

To evaluate the efficiency of a PMS, two measures were defined in [72]. The first called the board efficiency, denoted as $\eta_{\text{board}}$, is the ratio between the energy consumed by the functional circuits and the energy transferred from $C_{\text{temp}}$, in one cycle of TENG operation. The second called the total efficiency, denoted as $\eta_{\text{total}}$, is the ratio between the energy consumed by the functional circuits and the maximum energy a TENG device can deliver to a resistive load (with an optimized resistance), when the resistor is directly connected to the TENG.

It is reported that the PMS in [72] has a board efficiency $\eta_{\text{board}} = 90\%$ and a total efficiency $\eta_{\text{total}} = 59.8\%$. A similar but simpler PMS is presented in [85], where the switch J2 is replaced with a diode, as in a standard flyback converter, and the capacitor $C_{\text{Temp}}$ is absent. A notable difference as compared with [72] is the operation of the switch J1. Ideally, the switch is turned ON as the separation distance $x$ reaches the maximum or 0, and turned OFF before $x$ starts to change. It has the same intended operation as the switch in [52] but is connected with the TENG in series instead of in parallel. In the experiment, the intended function of the switch is implemented approximately with electronic devices, where a logic circuit detects the peak value of the rectified voltage and turns on a MOSFET immediately. Since a MOSFET needs a driver and the logic circuit needs steady power supply, the PMS will need additional power source, such as a battery, to be functional.

Another PMS is developed in [97] based on a buck converter, see Fig. 13. The switch J1 is implemented with a MOSFET and controlled by a comparator. As in [72], the switch is turned ON when the voltage $U_T$ reaches a reference value. Again, this PMS needs an additional power source to be functional. The total efficiency reported for this PMS is 80.4%. The buck converter topology is also used in [98], with an addition of a backflow-restraining diode between the rectifier and the switch.

A buck–boost converter-based PMS is developed in [99], as depicted in Fig. 14. The switch is controlled by a logic circuit based on the voltage across the storage capacitor $C_{\text{int,opt}}$ and the output voltage. The operation of the switch is similar to the other PMS. Similarly, additional power source is needed for the logic control unit and for driving the switch.

The total efficiency of the PMS in [99] is reported as 50%. It should be noted that the above PMS based on power converters all utilize a full wave rectifier for front end conversion.

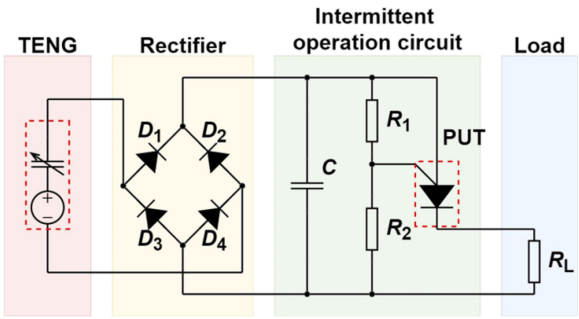


Fig. 15. PMS with a passive switch using PUT [100].

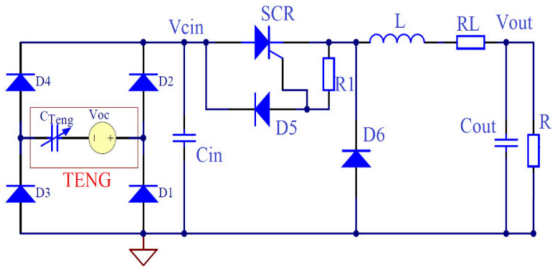


Fig. 16. Complete circuit of the PMS in [51].

## VI. Power Converter Topologies With Passive Electronic Switches

The power converter topologies presented in the previous section have been demonstrated to be effective for converting the pulsed output of the TENG to steady power supply while stepping down the high voltage to a level suitable for most applications. However, the limitation of these topologies has been observed recently. For the PMS discussed in Section V, there is one or more active switches implemented with MOSFETs, which are controlled by logic devices. Since MOSFET drivers and logic devices need external power supply, a PMS based on active switches is not able to fulfill the original purpose of developing self-powered systems with a TENG device. The mechanical switches discussed in Section III are passive, but they generally complicate the design of the TENG and are not as durable and reliable as electronic switches. To address these issues, PMS with passive electronic switches have been developed in the last two years in [51], [53], [100], [101].

The PMS presented in [100] utilizes a programmable unijunction transistor (PUT) to implement the switch, see Fig. 15. As the TENG is operated, the voltage across C (1 $\mu$F) increases until reaching 4 V. Then the PUT turns ON to transfer the energy from C to $R_L$ (1 $M\Omega$). When the capacitor voltage decreases to 0.5 V, the PUT turns OFF. The voltage across $R_L$ is intermittent and varies between 3.7 to 0.5 V when it is ON. This simple PMS was utilized to drive a stopwatch in [100]. The onboard efficiency from C to $R_L$ is reported as 89%.

The PMS in [100] is simple but the load voltage is not continuous. A more advanced PMS was developed in [51] to produce a continuous output by using a buck converter, which is similar to the one in Fig. 13, but the switch J1 is implemented with the combination of an SCR and a Zener diode. The complete circuit is shown in Fig. 16.

Here is a description of how the energy is transferred from the TENG to the load R, and how the SCR and the Zener diode D5 implement the function of the switch. For clarity, one cycle of energy transfer from the TENG to the load R is divided into five phases. Note that before the system starts, the voltage across $C_{in}$ is 0, and the SCR and the Zener diode do not conduct (equivalent to *the off state of* a *switch*).

*Phase 1*: After the TENG is agitated by mechanical force, charge is generated and stored in the capacitor $C_{\text{in}}$, causing an increase of $V_{C\text{in}}$.

*Phase 2*: As $V_{C\text{in}}$ exceeds the breakdown voltage of the Zener diode D5 + $V_{\text{out}}$, D5 starts to reverse conduct, injecting current to the gate of the SCR and triggering it to conduct (like the *turning on of a switch*), with the SCR's voltage rapidly decreasing to 0.

*Phase 3*: The SCR conducts. The energy stored in $C_{\text{in}}$ is transferred to the inductor *L* via a resonant mechanism, with $V_{C\text{in}}$ decreasing to 0 and D6 becomes forward biased.

*Phase 4*: The forward conduction of D6 locks $V_{C\text{in}}$ at around 0 and keeps the current through $C_{\text{in}}$ and the SCR at 0, which is equivalent to *turning off the switch* and getting ready for the next TENG charge. During this phase, the energy stored in the inductor *L* is transferred to $C_{\text{out}}$. This phase ends when the inductor current decreases to 0 and D6 stops conducting.

*Phase 5*: Energy in $C_{\text{out}}$ is transferred to the load *R*.

For interested readers, the LTspice model for the circuit in Fig. 16 is provided via the link at [79].

For the experimental system in [51], the TENG is subject to mechanical agitations of frequency ranging from 1 to 3 Hz. Phases 2, 3, 4 together take less than 1 ms, a very small fraction of the TENG's motion cycle. Phases 1 and 5 take most of a motion cycle and the previous phase 5 nearly completely overlaps with the next phase 1 (The TENG charges $C_{\text{in}}$ while $C_{\text{out}}$ discharges to R).

In the configuration in Fig. 16, the switch implemented with an SCR and a Zener diode perfectly suits the TENG's unique electrical property: pulsed charge with high peak voltage. In the experimental system, the peak voltage across $C_{\text{in}}$ after one cycle of TENG charge is around 500 V (for $C_{\text{in}}$ = 680 pF), much greater than the diode D6's forward voltage (about 1 V). For this reason, almost all energy stored in $C_{\text{in}}$ is transferred to *L* in phase 3 if an ideal SCR is used. Such a configuration would not be effective on other generators such as PENG and EMG, due to the low voltage across the output of the diode bridge.

In Fig. 17(a), a prototype of the PMS in [51] is pictured together with a TENG device in an experimental setup. The TENG device measures 7 cm square. It is activated by finger tapping. The oscilloscope in Fig. 17(a) shows the steady increase of the output voltage $V_{\text{out}}$ from 0 to a few volts after 16 s. The measured output voltage at 2 and 3 Hz frequency of finger tapping is shown in Fig. 17(b)–(d), where the green curve is $V_{C\text{in}}$ and the orange curve is $V_{\text{out}}$. Fig. 17(b) shows the transient response. Fig. 17(c) and (d) shows the steady state responses at 2 and 3 Hz. In the experimental circuit for generating Fig. 17, $C_{\text{in}}$ = 680 pF, $C_{\text{out}}$ = 47 $\mu$F, $L$ = 3.3 mH, and $R$ = 248 k$\Omega$. The steady state output power is 167 $\mu$W at 2 Hz TENG frequency and 209 $\mu$W at 3 Hz. The board efficiency is reported as 89.8%. However, it was later found out in [54] that there was

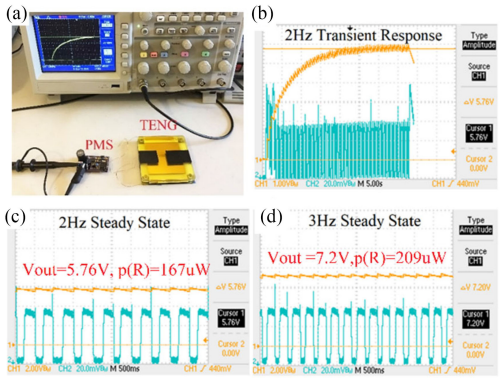


Fig. 17. (a) TENG and PMS prototype in an experiment setup; (b)–(d) Output voltage $V_{\text{out}}$ (orange) and $V_{C\text{in}}$(green) at 2 and 3 Hz TENG frequency.

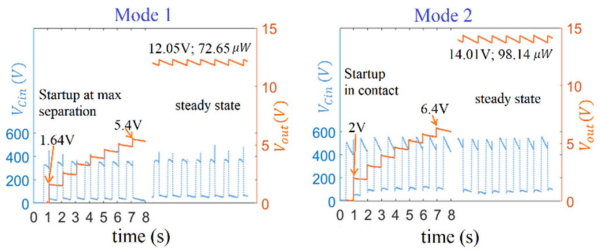


Fig. 18. Two modes of startup and steady state responses [54].

a misconception about the computation of the board efficiency and this measure may not be well defined, as will be explained below.

Further experiments with the TENG–PMS system revealed some fascinating interaction between the TENG and the PMS. An unusual steady state with about 30% higher output power than that in [51] was reported in [54]. Detailed investigation reveals that the TENG has more energy to offer than expected from the original design of the PMS. As the buck converter (in Fig. 16) transfers the energy stored in $C_{\text{in}}$ to the output capacitor $C_{\text{out}}$, the TENG acts as a capacitor in parallel with $C_{\text{in}}$, and contributes an additional amount of energy proportional to its capacitance. Since the internal capacitance $C_{\text{Teng}}$ is time varying and takes the maximum value when the two triboelectric surfaces are in contact, the optimal timing for energy transfer from $C_{\text{in}}$ to $C_{\text{out}}$ is when the separation distance approaches 0.

Fig. 18 shows the two modes of startup and steady state responses with a 2 $M\Omega$ load and 1 Hz TENG frequency. For mode 1, as observed in [51], $C_{\text{in}}$ transfers energy to $C_{\text{out}}$ when the separation distance is near the maximum. For mode 2, the energy transfer occurs when the separation distance is nearly 0. The output power for mode 2 is 98.14 $\mu W$ , about 35% higher than that for mode 1 (72.65 $\mu W$).

For both modes 1 and 2, there is direct energy transfer from the TENG device (without going through $C_{\text{in}}$), which is not considered in the computation of the board efficiency in [51] and previous works. Due to this additional energy contribution from the TENG, the board efficiency used in previous works may not be well defined. Since any additional sensor directly connected to a TENG will disrupt and reduce its energy generation, it is difficult to measure the total energy generated by a TENG device by experiment. For this reason, [54] used simulation data to

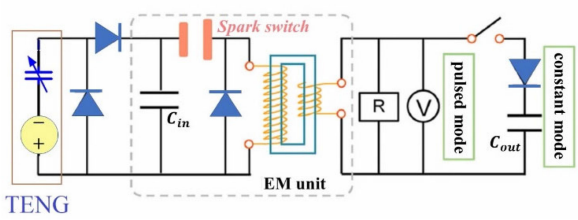


Fig. 19. A PMS with a spark switch [53].

evaluate the total energy generation of the TENG and the energy consumption by every device. For mode 1, the energy consumed by the load is about 70% of the total energy generated by the TENG; and for mode 2, about 71%–74%, much less than the board efficiency reported in [51] and previous works. This is partly due to the power loss in the bridge rectifier, and partly due to the unaccounted direct energy transfer from the TENG to the buck converter.

In [53], another PMS with passive switch is presented, where a transformer is used to step down the TENG's high voltage, rectified by a halfwave bridge (see Fig. 19).

This PMS has a unique auto spark switch, which is triggered by a 7500 V voltage across $C_{\text{in}}$. As the TENG is mechanically agitated, it stores energy in $C_{\text{in}}$ via the halfwave bridge. As the voltage across $C_{\text{in}}$ reaches 7500 V, the spark switch is closed and the energy stored in $C_{\text{in}}$ is instantly transferred to the primary side of the transformer, which, in turn, is transferred to the secondary side, and then to $C_{\text{out}}$. The manual switch at the top right of the circuit chooses between two modes of applications. It stays either open or closed for each application.

To maximize the energy extracted from the TENG and to ensure the turn ON of the spark switch, $C_{\text{in}}$ has a low capacitance around 25 pF. As claimed in [53], the advantages of the spark switch include low leakage current and high stability.

The operation principle of the PMS in Fig. 19 is simple and straightforward. The challenges are mostly on the construction of the spark switch, the transformer, the diodes, and $C_{\text{in}}$, which all need to sustain a 7500 V voltage. In [53], the transformer is custom made with a high voltage skeleton to withstand the high voltage. Another limitation is that the PMS requires a humidity below 60%. Although there are some technical challenges and limitations for the PMS in [53], the results demonstrate the energy generation capability of the TENG. The TENG device used in [53] measures 10 cm square. The output power of the PMS on a 200k resistor is 1.1 mW at 1 Hz TENG frequency and 2.9 mW at 3 Hz. The onboard efficiency form $C_{\text{in}}$ to $C_{\text{out}}$ at 1 Hz is reported as 86.7%, and the total efficiency is 78.5%.

The spark switch was also used in [101] to construct two PMS, one based on a buck converter, one based on a flyback converter, see Fig. 20. The main objective in [101] is the optimization of the inductor in the converters.

A summary of the existing technologies for TENG PMS, as discussed above, is presented in Table I. Since the design objectives and the load types have been changed over the past decade, the output specifications are not unified. Therefore, we use column 2 to specify the output voltage and load type, and the last column to provide some information on the main objectives of the design, or some key specifications for the output. It should

TABLE I
SUMMARY OF EXISTING TECHNOLOGIES

| Reference work | Output voltage/ load type | Rectifying stage | dc-dc converter | Type of switch | Notes |
|---|---|---|---|---|---|
| [52], [80] | AC/resistor | no | no | mechanical | design objective: boost peak output power |
| [81]-[83] | AC/resistor | no | no | electrostatic, air discharge | design objective: boost peak output power |
| [88] | DC/capacitor | Full wave | no | mechanical | design objective: increase saturation voltage |
| [77], [89] | DC/capacitor | Full wave, half wave, Bennet's doubler | no | diode | compare charging curves of 3 rectifying methods, exponential growth in Bennet's doubler |
| [95] | AC/capacitor | no | switched capacitor | mechanical | 2 capacitors, pulsed output, peak < 50V, 1.74$\mu$W at 1Hz |
| [94] | DC/resistor | Full wave | switched capacitor | mechanical | up to 8 capacitors, pulsed output, peak 15 – 60V |
| [96] | DC/resistor | Half wave | switched capacitor | diode /mechanical | fractal design up to 96 capacitors, constant output, < 17V, 37mW/$m^2$ at 1Hz |
| [72], [85] | DC/resistor | Full wave | flyback | MOSFET | constant output, < 20 V,0.2mW |
| [97] | DC/resistor | Full wave | buck | MOSFET | constant output < 4 V, 9 $\mu$W at 1Hz |
| [99] | DC/resistor | Full wave | buck-boost | MOSFET | constant output < 20V, 52.5mW, at 170rpm |
| [100] | DC/resistor | Full wave | no | PUT | pulsed output < 4V, 6.7 $\mu$W at 1Hz |
| [51], [54] | DC/resistor | Full wave | buck | SCR | constant output < 14 V, 98 $\mu$W at 1Hz |
| [53] | DC/resistor | Half wave | transformer | spark | constant output < 20 V, 1.1 mW at 1Hz |
| [101] | DC/resistor | Half wave | buck, flyback | spark | constant output < 25V 0.89 mW at 1 Hz |

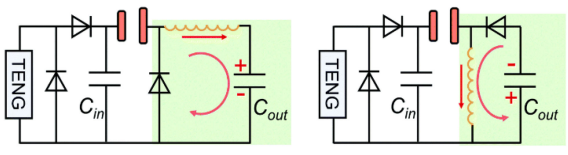


Fig. 20. PMS in [101] based on a buck converter (A) and a flyback converter (B) with spark switch.

be noted that the numbers should only be used as a reference, not for comparison, since the TENG devices used in the cited works are different in terms of size, material, construction, etc., and the output types are different (ac, dc, constant, pulsed). The energy efficiency numbers are not included in the table, to avoid controversy, since some of them may not be well defined, as explained earlier.

## VII. PERSPECTIVES ON TENG'S POWER MANAGEMENT

The existing PMS reviewed in the above sections provide a strong proof of concept for self-powered systems based on TENGs. However, before the self-powered devices enter the market and benefit the daily lives of humankind, substantial research efforts are required to address various issues which may arise from applications, such as maximum output power, maximum energy conversion efficiency, small size, durability, fast charging, energy storage capability, and other user functions.

### *A. Enhancement of Output Power*

The maximum output power in [53] is a little above 1 mW at 1-Hz TENG frequency (comparable to human walking), for a TENG device measuring 10 cm $\times$ 10 cm. This amount of output power is sufficient to supply many health monitors, such as the blood pressure monitoring system in [102], which runs on as little as 56 $\mu$ W. However, a smart phone may consume as much as 1 W when Google map is running [103] and 0.3 W when

sending a message [104]. To expand the applications of self-powered systems, joint efforts have been made by scientists and engineers from different fields. On one hand, continuous efforts have been made to reduce the power consumption of electronic devices [9], [21], [29], [30], for example, an ultralow-power cellphone has been developed in [105], which runs on as low as 3.48 $\mu$W. On the other hand, there has been ongoing research on increasing TENG's output power and performance, from materials optimization to structural design [59]–[63], [106], [107]. For power electronics engineers, our expertise can be contributed to the development of high-performance and high-efficiency PMS that extracts the maximum output power from the TENGs with ultra-low or "zero" energy consumption.

Although TENGs have been investigated by scientists and engineers for more than nine years in thousands of publications [59], their energy generation mechanism and potential are yet to be fully explored and exploited [5]. For a direct resistive load or a capacitive load (without any switch), the energy delivered to it for each motion cycle can be computed analytically [71]. However, it has been discovered that the energy extraction from a TENG can be significantly boosted by designing switched power flow paths, for example, by placing a switch in parallel with the TENG and turning on the switch when $C_{\text{Teng}}$ reaches its maximum or minimum, and turning it OFF before $C_{\text{Teng}}$ starts to change. It is likely that there exist other switching topologies which will further boost the energy extraction.

Other energy harvesters, such as solar panels and piezoelectric generators, have well-defined maximum power and there exist strategies to extract the maximum power (see [49] for PENGs). For TENGs, the maximum power is unknown or not well defined yet.

The PMS based on Bennet's doubler in [77] and [89] seems to indicate that the maximum energy extraction from the TENG is unlimited, or only to be limited by the voltage ratings of the diodes and the capacitors. The energy extraction from the TENG increases exponentially after many motion cycles, owing to the nonlinear internal capacitance of the TENG. Although the objective in [77] is to store energy in a small capacitor, the mechanism of Bennet's doubler and the nonlinearity of $C_{\text{Teng}}$ may be explored for building a practical power supply. The energy extracted and stored in a capacitor not only depends on the capacitance, but also the initial condition at the beginning of a motion cycle. What is the optimal capacitance? What is the ideal initial condition that can be practically reached and maintained while supplying a load? How to design a circuit to transfer the energy stored in the capacitor to a load? These questions may lead to interesting and challenging research tasks and in-depth investigation into TENG's energy generation capability and effective extraction strategies.

As a unique energy harvester, the TENG's fascinating electrical property was demonstrated in [54], via its interaction with a PMS. The same TENG combined with a PMS system produced two different modes of steady-state output behavior. The first mode is the usual output as observed in [51], which is easy to produce. The second mode's output power is 30% higher than that of the first one, but it is somewhat tricky to produce as it requires manipulating the TENG's motion. One interesting research problem is to design some control circuit to bring the system from the first mode to the second mode and stabilize the system at the second mode.

These examples demonstrate that there are many questions to be answered about TENG's energy generation capability, and there is a great potential to boost the output power by exploring the unique electrical properties of the TENG, especially the nonlinear capacitance.

Another opportunity to boost the output power and efficiency of a PMS comes from the device level. The analysis of power consumption of the devices in [54] shows a modest efficiency of around 74%, and that the SCR and the diodes consume a significant portion of the generated energy. Note that a unique feature of TENGs is that they generate electricity with very high voltage (e.g., 1000 V) but low power (e.g., 1 mW). The semiconductor devices used in the prototype PMS must satisfy a voltage rating above 600 V. In the current semiconductor market, the devices with such a high voltage rating usually handle at least a few hundred watts of power, with a current rating greater than a few amperes, in contrast to the milliampere or microampere range in the PMS. The redundant capacity for handling much higher current than needed may be traded for much-reduced size, lower leakage current in the diodes, lower forward diode voltage, and faster turn-on of SCR, which will lead to a smaller inductor and reduced power loss. This will motivate the design of custom semiconductor devices that are specially tailored for handling the low power flow of the TENG PMS.

### *B. Regulating Output Voltage or Current*

The output voltage in the current PMS designs depends on the resistive load, which is not regulated. When driving sensitive electronic devices, the output voltage should be a constant such as 3 or 5 V, regardless of the load. One straightforward solution is to use another dc–dc converter to regulate the voltage or current.

The challenge in this task is the low-power output of the TENG and of the power converter stage, usually around a few milli or micro watts. For this reason, some elements in traditional power converters, such as MOSFET driver, pulse generator, pulse-width-modulation, and logic control ICs, should be avoided. The concept of self-oscillation may be explored to minimize the power loss. In a recent paper [108], an LED driver based on a self-oscillation boost converter is developed for high efficiency, low component count, and small size. One controller IC is used to combine the functions of controller, pulse generator, pulse width modulation, and MOSFET driver based on a self-oscillation mechanism. The self-oscillation concept maybe further explored in order to reduce power loss, cost, and size. There may also exist a solution of using only one stage of power conversion for compact size and low power loss. Preliminary investigation shows that a JFET may be used to regulate the output voltage with low power loss. Further research needs to be conducted to achieve maximum load current at the fixed output voltage.

### *C. Energy Storage in a Supercapacitor or Battery*

When the instantaneous output power harvested by the TENG/PMS system is less than what is needed by some applications, an energy storage device, such as a supercapacitor,

will make it possible to serve those applications. With an energy storage device, the energy generated during exercise can also be saved for later use. The desired functions of the PMS will include 1) when mechanical energy is abundant, supply power to electronic device directly while saving extra energy to an energy storage element. 2) When mechanical energy is not present or not sufficient, supply power to electronic device using the energy from the storage unit. For supplying power to conventional electronic devices, the output voltage is usually between 3 and 5 V. To maximize energy storage, the design objective is to maximize the current flowing into the storage device.

### *D. PMS for Hybrid Nanogenerators*

TENGs have emerged as the most powerful and most promising technology for harvesting biomechanical energy, which is generally of low frequency. Recent efforts have been devoted to the integration of TENG with other types of harvesters to expand the power of the TENG and its application range, see e.g., [109]–[112]. A review of the progress of hybrid nanogenerators based on TENG can be found in [113]. In the nano energy community, almost all efforts have been devoted to the design of hybrid generators for increased power density. There is inadequate research activity on the development of PMS for these hybrid generators. Simple parallel strategies for the integration of the outputs of hybrid nano-generators were presented in [114] and [115]. The parallel connections in the existing works are very crude and not efficient. However, it reveals research opportunities for power electronics engineers to significantly improve the total output power of hybrid nanogenerators with advanced PMS that can effectively integrate several outputs which have very different electrical properties. The different voltage levels and the different internal properties of the nanogenerators require the energy of each generator to be processed separately by its respective PMS before being transferred to the same energy storage unit. In contrast to TENG's buck-converter-based PMS, the PMS for PENG and EMG are usually based on boost converters due to the low output voltage for low-frequency biomechanical activities. Resources for addressing the above issues can be found in the literature on multi-input-single-output power converters. In [116]–[118], various topologies are presented for integrating power sources of high/low voltage levels by combining a buck converter and a boost converter. These topologies can be potentially adapted for the power management of hybrid nanogenerators. However, challenges will be expected due to the differences in the electrical properties of the nanogenerators and the need for self-powered PMS.

## VIII. Conclusion

Recent progress in the power management for TENGs has presented a strong proof of concept for self-powered systems with TENGs as the energy harvesting unit. It also demonstrates the critical and indispensable role of power electronics in the power management of nanogenerators for self-powered systems. This review is intended to introduce the problem of power management of TENGs to the electrical engineering community and to present some promising research opportunities arising from TENG's very unique electrical properties. Over the years, numerous research works have proposed various circuit topologies for the design of switched power flow paths including short-circuiting the TENG when the internal capacitance is maximum or minimum, changing the connection of external capacitors between series and parallel, using different rectifiers such as halfwave, full wave, and Bennet's doubler, and using different power converters such as buck and flyback. However, the maximum energy generation capability of TENG as well as its optimal energy extraction strategy remains unclear. To this end, this review is aimed at informing and evoking the interest of power electronics engineers and researchers in investigating these meaningful and intriguing problems.

## References


[1] F.-R. Fan, Z.-Q. Tian, and Z. L. Wang, "Flexible triboelectric generator," *Nano Energy*, vol. 1, no. 2, pp. 328–334, 2012.

[2] F.-R. Fan, L. Lin, G. Zhu, W. Wu, R. Zhang, and Z. L. Wang, "Transparent triboelectric nanogenerators and self-powered pressure sensors based on micropatterned plastic films," *Nano Lett.*, vol. 12, no. 6, pp. 3109–3114, 2012.

[3] Z. L. Wang and J. Song, "Piezoelectric nanogenerators based on zinc oxide nanowire arrays," *Science*, vol. 312, no. 5771, pp. 242–246, 2006.

[4] Z. L. Wang, "Triboelectric nanogenerators as new energy technology and self-powered sensors–Principles, problems and perspectives," *Faraday Discuss.*, vol. 176, pp. 447–458, 2015.

[5] Z. L. Wang, J. Chen, and L. Lin, "Progress in triboelectric nanogenerators as a new energy technology and self-powered sensors," *Energy Environ. Sci.*, vol. 8, no. 8, pp. 2250–2282, 2015.

[6] Z. L. Wang, "Nanogenerators, self-powered systems, blue energy, piezotronics and piezo-phototronics–a recall on the original thoughts for coining these fields," *Nano Energy*, vol. 54, pp. 477–483, 2018.

[7] J. Kymissis, C. Kendall, J. Paradiso, and N. Gershenfeld, "Parasitic power harvesting in shoes," in *Proc. Dig. Papers. 2nd Int. Symp. Wearable Comput.*, 1998, pp. 132–139.

[8] R. Riemer and A. Shapiro, "Biomechanical energy harvesting from human motion: Theory, state of the art, design guidelines, and future directions," *J. NeuroEng. Rehabil.*, vol. 8, no. 1, 2011, Art. no. 22.

[9] T. Starner, "Human-powered wearable computing," *IBM Syst. J.*, vol. 35, no. 3.4, pp. 618–629, 1996.

[10] A. D. Kuo, "Harvesting energy by improving the economy of human walking," *Science*, vol. 309, no. 5741, 2005, Art. no. 1686.

[11] L. C. Rome, L. Flynn, E. M. Goldman, and T. D. Yoo, "Generating electricity while walking with loads," *Science*, vol. 309, no. 5741, 2005, Art. no. 1725.

[12] Z. Liu, H. Li, B. Shi, Y. Fan, Z. L. Wang, and Z. Li, "Wearable and implantable triboelectric nanogenerators," *Adv. Funct. Mater.*, vol. 29, no. 20, 2019, Art. no. 1808820, doi: 10.1002/adfm.201808820.

[13] A. Khaligh, Z. Peng, W. Xiaochun, and X. Yang, "A hybrid energy scavenging topology for human-powered mobile electronics," in *Proc. 34th Annu. Conf. IEEE Ind. Electron.*, 2008, pp. 448–453.

[14] S. Patel, H. Park, P. Bonato, L. Chan, and M. Rodgers, "A review of wearable sensors and systems with application in rehabilitation," *J. NeuroEng. Rehabil.*, vol. 9, no. 1, 2012, Art. no. 21.

[15] D. Ma, G. Lan, M. Hassan, W. Hu, and S. K. Das, "Sensing, computing, and communications for energy harvesting iots: A survey," *IEEE Commun. Surv. Tut.*, vol. 22, no. 2, pp. 1222–1250, 2020.

[16] C. Dagdeviren, Z. Li, and Z. L. Wang, "Energy harvesting from the animal/human body for self-powered electronics," *Annu. Rev. Biomed. Eng.*, vol. 19, no. 1, pp. 85–108, 2017.

[17] J. L. Gonz *et al.*, "Human powered piezoelectric batteries to supply power to wearable electronic devices," *Int. J. Soc. Mater. Eng. Resour.*, vol. 10, no. 1, pp. 34–40, 2002.

[18] S. Khalid, I. Raouf, A. Khan, N. Kim, and H. S. Kim, "A review of human-powered energy harvesting for smart electronics: Recent progress and challenges," *Int. J. Precis. Eng. Manuf.-Green Technol.*, vol. 6, no. 4, pp. 821–851, 2019.

[19] M. Shi and H. Wu, "Applications in internet of things and artificial intelligence," in *Flexible and Stretchable Triboelectric Nanogenerator Devices: Toward Self-Powered Systems*. Hoboken, NJ, USA: Wiley, 2019, pp. 359–378.

[20] H. Sun, M. Yin, W. Wei, J. Li, H. Wang, and X. Jin, "MEMS based energy harvesting for the internet of things: A survey," *Microsyst. Technol.*, vol. 24, no. 7, pp. 2853–2869, 2018.

[21] R. Hinchet and S.-W. Kim, "Wearable and implantable mechanical energy harvesters for self-powered biomedical systems," *ACS Nano*, vol. 9, no. 8, pp. 7742–7745, 2015.

[22] V. S. Mallela, V. Ilankumaran, and N. S. Rao, "Trends in cardiac pacemaker batteries," *Indian Pacing Electrophysiol. J.*, vol. 4, no. 4, pp. 201–212, 2004.

[23] J. H. Park, C. Wu, S. Sung, and T. W. Kim, "Ingenious use of natural triboelectrification on the human body for versatile applications in walking energy harvesting and body action monitoring," *Nano Energy*, vol. 57, pp. 872–878, 2019.

[24] J. M. Donelan, Q. Li, V. Naing, J. A. Hoffer, D. J. Weber, and A. D. Kuo, "Biomechanical energy harvesting: Generating electricity during walking with minimal user effort," *Science*, vol. 319, no. 5864, 2008, Art. no. 807.

[25] N. G. Elvin and A. A. Elvin, "Vibrational energy harvesting from human gait," *IEEE/ASME Trans. Mechatronics*, vol. 18, no. 2, pp. 637–644, Apr. 2013.

[26] G. Wang, C. Luo, H. Hofmann, and L. Rome, "Power electronic circuitry for energy harvesting backpack," in *Proc. IEEE Energy Convers. Congr. Expo.*, 2009, pp. 3544–3549.

[27] Q. Li, V. Naing, and J. M. Donelan, "Development of a biomechanical energy harvester," *J. NeuroEng. Rehabil.*, vol. 6, no. 1, 2009, Art. no. 22.

[28] E. Häsler, L. Stein, and G. Harbauer, "Implantable physiological power supply with PVDF film," *Ferroelectrics*, vol. 60, no. 1, pp. 277–282, 1984.

[29] S. Chandrasekaran *et al.*, "Micro-scale to nano-scale generators for energy harvesting: Self powered piezoelectric, triboelectric and hybrid devices," *Phys. Rep.*, vol. 792, pp. 1–33, 2019.

[30] Y. Hu and Z. L. Wang, "Recent progress in piezoelectric nanogenerators as a sustainable power source in self-powered systems and active sensors," *Nano Energy*, vol. 14, pp. 3–14, 2015.

[31] J. Chen *et al.*, "Networks of triboelectric nanogenerators for harvesting water wave energy: A potential approach toward blue energy," *ACS Nano*, vol. 9, no. 3, pp. 3324–3331, 2015.

[32] B. Chen, Y. Yang, and Z. L. Wang, "Scavenging wind energy by triboelectric nanogenerators," *Adv. Energy Mater.*, vol. 8, no. 10, 2018, Art. no. 1702649.

[33] U. Khan and S.-W. Kim, "Triboelectric nanogenerators for blue energy harvesting," *ACS Nano*, vol. 10, no. 7, pp. 6429–6432, 2016.

[34] X. Liang *et al.*, "Triboelectric nanogenerator networks integrated with power management module for water wave energy harvesting," *Adv. Funct. Mater.*, vol. 29, no. 41, 2019, Art. no. 1807241.

[35] Z.-H. Lin, G. Cheng, X. Li, P.-K. Yang, X. Wen, and Z. Wang, "A multi-layered interdigitative-electrodes-based triboelectric nanogenerator for harvesting hydropower," *Nano Energy*, vol. 15, pp. 256–265, 2015.

[36] Z. L. Wang, T. Jiang, and L. Xu, "Toward the blue energy dream by triboelectric nanogenerator networks," *Nano Energy*, vol. 39, pp. 9–23, 2017.

[37] Z. Wen *et al.*, "Harvesting broad frequency band blue energy by a triboelectric–electromagnetic hybrid nanogenerator," *ACS Nano*, vol. 10, no. 7, pp. 6526–6534, 2016.

[38] Y. Yang *et al.*, "Triboelectric nanogenerator for harvesting wind energy and as self-powered wind vector sensor system," *ACS Nano*, vol. 7, no. 10, pp. 9461–9468, 2013.

[39] L. Zhang *et al.*, "Lawn structured triboelectric nanogenerators for scavenging sweeping wind energy on rooftops," *Adv. Mater.*, vol. 28, no. 8, pp. 1650–1656, 2016.

[40] H. Askari, A. Khajepour, M. B. Khamesee, Z. Saadatnia, and Z. L. Wang, "Piezoelectric and triboelectric nanogenerators: Trends and impacts," *Nano Today*, vol. 22, pp. 10–13, 2018.

[41] X. Wang *et al.*, "Harvesting ambient vibration energy over a wide frequency range for self-powered electronics," *ACS Nano*, vol. 11, no. 2, pp. 1728–1735, 2017.

[42] Y. Zi, H. Guo, Z. Wen, M.-H. Yeh, C. Hu, and Z. L. Wang, "Harvesting low-frequency ($<$ 5 Hz) irregular mechanical energy: A possible killer application of triboelectric nanogenerator," *ACS Nano*, vol. 10, no. 4, pp. 4797–4805, 2016.

[43] A. Ahmed *et al.*, "Environmental life cycle assessment and techno-economic analysis of triboelectric nanogenerators," *Energy Environ. Sci.*, vol. 10, no. 3, pp. 653–671, 2017, doi: 10.1039/C7EE00158D.

[44] Q. Liang *et al.*, "Recyclable and green triboelectric nanogenerator," *Adv. Mater.*, vol. 29, no. 5, 2017, Art. no. 1604961.

[45] S. Boisseau, P. Gasnier, M. Gallardo, and G. Despesse, "Self-starting power management circuits for piezoelectric and electret-based electrostatic mechanical energy harvesters," *J. Phys., Conf. Ser.*, vol. 476, 2013, Art. no. 012080.

[46] M. Dini, M. Filippi, M. Tartagni, and A. Romani, "A nano-power power management IC for piezoelectric energy harvesting applications," in *Proc. 9th Conf. Ph.D. Res. Microelectron. Electron.*, 2013, pp. 269–272.

[47] R. D. hulst, T. Sterken, R. Puers, G. Deconinck, and J. Driesen, "Power processing circuits for piezoelectric vibration-based energy harvesters," *IEEE Trans. Ind. Electron.*, vol. 57, no. 12, pp. 4170–4177, Dec. 2010.

[48] N. Kong, T. Cochran, D. S. Ha, H. Lin, and D. J. Inman, "A self-powered power management circuit for energy harvested by a piezoelectric cantilever," in *Proc. 25th Annu. IEEE Appl. Power Electron. Conf. Expo.*, 2010, pp. 2154–2160.

[49] N. Kong and D. S. Ha, "Low-power design of a Self-powered piezoelectric energy harvesting system with maximum power point tracking," *IEEE Trans. Power Electron.*, vol. 27, no. 5, pp. 2298–2308, May 2012.

[50] X. Cheng, W. Tang, Y. Song, H. Chen, H. Zhang, and Z. L. Wang, "Power management and effective energy storage of pulsed output from triboelectric nanogenerator," *Nano Energy*, vol. 61, pp. 517–532, 2019.

[51] W. Harmon, D. Bamgboje, H. Guo, T. Hu, and Z. L. Wang, "Self-driven power management system for triboelectric nanogenerators," *Nano Energy*, vol. 71, 2020, Art. no. 104642.

[52] G. Cheng, Z.-H. Lin, L. Lin, Z.-L. Du, and Z. L. Wang, "Pulsed nanogenerator with huge instantaneous output power density," *ACS Nano*, vol. 7, no. 8, pp. 7383–7391, 2013.

[53] Z. Wang *et al.*, "Ultrahigh electricity generation from low-frequency mechanical energy by efficient energy management," *Joule*, vol. 5, no. 2, pp. 441–455, 2021.

[54] W. Harmon, H. Guo, D. Bamgboje, T. Hu, and Z. L. Wang, "Timing strategy for boosting energy extraction from triboelectric nanogenerators," *Nano Energy*, vol. 85, 2021, Art. no. 105956.

[55] G. Zhu *et al.*, "Toward large-scale energy harvesting by a nanoparticle-enhanced triboelectric nanogenerator," *Nano Lett.*, vol. 13, no. 2, pp. 847–853, 2013.

[56] S. Wang, L. Lin, and Z. L. Wang, "Nanoscale triboelectric-effect-enabled energy conversion for sustainably powering portable electronics," *Nano Lett.*, vol. 12, no. 12, pp. 6339–6346, 2012.

[57] B. Meng *et al.*, "A transparent single-friction-surface triboelectric generator and self-powered touch sensor," *Energy Environ. Sci.*, vol. 6, no. 11, pp. 3235–3240, 2013, doi: 10.1039/C3EE42311E.

[58] S. Wang, Y. Xie, S. Niu, L. Lin, and Z. L. Wang, "Freestanding triboelectric-layer-based nanogenerators for harvesting energy from a moving object or human motion in contact and non-contact modes," *Adv. Mater.*, vol. 26, no. 18, pp. 2818–2824, 2014.

[59] T. Cheng, Q. Gao, and Z. L. Wang, "The current development and future outlook of triboelectric nanogenerators: A survey of literature," *Adv. Mater. Technol.*, vol. 4, no. 3, 2019, Art. no. 1800588.

[60] X. Cheng *et al.*, "Wide range fabrication of wrinkle patterns for maximizing surface charge density of a triboelectric nanogenerator," *J. Microelectromech. Syst.*, vol. 27, no. 1, pp. 106–112, 2018.

[61] M. Ma *et al.*, "Development, applications, and future directions of triboelectric nanogenerators," *Nano Res.*, vol. 11, no. 6, pp. 2951–2969, Jun. 2018.

[62] M. A. Parvez Mahmud, N. Huda, S. H. Farjana, M. Asadnia, and C. Lang, "Recent advances in nanogenerator-driven self-powered implantable biomedical devices," *Adv. Energy Mater.*, vol. 8, no. 2, 2018, Art. no. 1701210.

[63] W. Paosangthong, R. Torah, and S. Beeby, "Recent progress on textile-based triboelectric nanogenerators," *Nano Energy*, vol. 55, pp. 401–423, 2019.

[64] W. G. Kim *et al.*, "Triboelectric nanogenerator: Structure, mechanism, and applications," *ACS Nano*, vol. 15, no. 1, pp. 258–287, 2021.

[65] D. Liu, L. Zhou, Z. L. Wang, and J. Wang, "Triboelectric nanogenerator: From alternating current to direct current," *Science*, vol. 24, no. 1, 2021, Art. no. 102018.

[66] W. Liu, Z. Wang, and C. Hu, "Advanced designs for output improvement of triboelectric nanogenerator system," *Mater. Today*, vol. 45, pp. 93–119, 2021.

[67] H. Zou *et al.*, "Quantifying the triboelectric series," *Nature Commun.*, vol. 10, no. 1, pp. 1–9, 2019.

[68] C. Wu, A. C. Wang, W. Ding, H. Guo, and Z. L. Wang, "Triboelectric nanogenerator: A foundation of the energy for the new era," *Adv. Energy Mater.*, vol. 9, no. 1, 2019, Art. no. 1802906.

[69] H. Yang, F. R. Fan, Y. Xi, and W. Wu, "Design and engineering of high-performance triboelectric nanogenerator for ubiquitous unattended devices," *EcoMat*, vol. 3, no. 2, 2021, Art. no. 12093.

[70] S. Niu *et al.*, "Theoretical study of contact-mode triboelectric nanogenerators as an effective power source," *Energy Environ. Sci.*, vol. 6, no. 12, pp. 3576–3583, 2013.

[71] S. Niu and Z. L. Wang, "Theoretical systems of triboelectric nanogenerators," *Nano Energy*, vol. 14, pp. 161–192, 2015.

[72] S. Niu, X. Wang, F. Yi, Y. S. Zhou, and Z. L. Wang, "A universal self-charging system driven by random biomechanical energy for sustainable operation of mobile electronics," *Nature Commun.*, vol. 6, 2015, Art. no. 8975.

[73] S. Niu, Y. Liu, Y. S. Zhou, S. Wang, L. Lin, and Z. L. Wang, "Optimization of triboelectric nanogenerator charging systems for efficient energy harvesting and storage," *IEEE Trans. Electron Devices*, vol. 62, no. 2, pp. 641–647, Feb. 2015.

[74] S. Niu *et al.*, "Theory of sliding-mode triboelectric nanogenerators," *Adv. Mater.*, vol. 25, no. 43, pp. 6184–6193, 2013.

[75] S. Niu *et al.*, "Theoretical investigation and structural optimization of single-electrode triboelectric nanogenerators," *Adv. Funct. Mater.*, vol. 24, no. 22, pp. 3332–3340, 2014.

[76] S. Niu *et al.*, "Simulation method for optimizing the performance of an integrated triboelectric nanogenerator energy harvesting system," *Nano Energy*, vol. 8, pp. 150–156, 2014.

[77] A. Ghaffarinejad *et al.*, "A conditioning circuit with exponential enhancement of output energy for triboelectric nanogenerator," *Nano Energy*, vol. 51, pp. 173–184, 2018.

[78] W. Harmon, "A power management system for triboelectric nanogenerators," Ph.D. dissertation, Univ. Massachusetts Lowell, Lowell, MA, USA, 2021.

[79] Simulation files for TENG and PMS. [Online]. Available: https://drive.google.com/drive/folders/1MyljpUdLhKejsjl1b8s5IpXwLhegZJt4?usp=sharing

[80] H. Qin *et al.*, "High energy storage efficiency triboelectric nanogenerators with unidirectional switches and passive power management circuits," *Adv. Funct. Mater.*, vol. 28, no. 51, 2018, Art. no. 1805216.

[81] H. Qin *et al.*, "A universal and passive power management circuit with high efficiency for pulsed triboelectric nanogenerator," *Nano Energy*, vol. 68, 2020, Art. no. 104372.

[82] J. Yang *et al.*, "Managing and optimizing the output performances of a triboelectric nanogenerator by a self-powered electrostatic vibrator switch," *Nano Energy*, vol. 46, pp. 220–228, 2018.

[83] G. Cheng *et al.*, "Managing and maximizing the output power of a triboelectric nanogenerator by controlled tip–electrode air-discharging and application for UV sensing," *Nano Energy*, vol. 44, pp. 208–216, 2018.

[84] Y. Zi, S. Niu, J. Wang, Z. Wen, W. Tang, and Z. L. Wang, "Standards and figure-of-merits for quantifying the performance of triboelectric nanogenerators," *Nature Commun.*, vol. 6, no. 1, pp. 1–8, 2015.

[85] X. Cheng *et al.*, "High efficiency power management and charge boosting strategy for a triboelectric nanogenerator," *Nano Energy*, vol. 38, pp. 438–446, 2017.

[86] X. Nan, C. Zhang, C. Liu, M. Liu, Z. L. Wang, and G. Cao, "Highly efficient storage of pulse energy produced by triboelectric nanogenerator in Li3V2(PO4)3/C cathode li-ion batteries," *ACS Appl. Mater. Interfaces*, vol. 8, no. 1, pp. 862–870, 2016.

[87] X. Pu, W. Hu, and Z. L. Wang, "Toward wearable self-charging power systems: The integration of energy-harvesting and storage devices," *Small*, vol. 14, no. 1, 2018, Art. no. 1702817.

[88] Y. Zi *et al.*, "Effective energy storage from a triboelectric nanogenerator," *Nature Commun.*, vol. 7, no. 1, pp. 1–8, 2016.

[89] H. Zhang, Y. Lu, A. Ghaffarinejad, and P. Basset, "Progressive contact-separate triboelectric nanogenerator based on conductive polyurethane foam regulated with a Bennet doubler conditioning circuit," *Nano Energy*, vol. 51, pp. 10–18, 2018.

[90] X. Xia, H. Wang, P. Basset, Y. Zhu, and Y. Zi, "Inductor-free output multiplier for power promotion and management of triboelectric nanogenerators toward self-powered systems," *ACS Appl. Mater. Interfaces*, vol. 12, no. 5, pp. 5892–5900, 2020.

[91] H. Wang, J. Zhu, T. He, Z. Zhang, and C. Lee, "Programmed-triboelectric nanogenerators—A multi-switch regulation methodology for energy manipulation," *Nano Energy*, vol. 78, 2020, Art. no. 105241.

[92] A. Ioinovici, "Switched-capacitor power electronics circuits," *IEEE Circuits Syst. Mag.*, vol. 1, no. 3, pp. 37–42, 2001.

[93] B. Axelrod, Y. Berkovich, S. Tapuchi, and A. Ioinovici, "Single-Stage single-switch switched-capacitor buck/buck-boost-type converter," *IEEE Trans. Aerosp. Electron. Syst.*, vol. 45, no. 2, pp. 419–430, Apr. 2009.

[94] W. Tang, T. Zhou, C. Zhang, F. R. Fan, C. B. Han, and Z. L. Wang, "A power-transformed-and-managed triboelectric nanogenerator and its applications in a self-powered wireless sensing node," *Nanotechnology*, vol. 25, no. 22, 2014, Art. no. 225402.

[95] Y. Zi *et al.*, "An inductor-free auto-power-management design built-in triboelectric nanogenerators," *Nano Energy*, vol. 31, pp. 302–310, 2017.

[96] W. Liu *et al.*, "Switched-capacitor-convertors based on fractal design for output power management of triboelectric nanogenerator," *Nature Commun.*, vol. 11, no. 1, p. 1883, 2020.

[97] F. Xi *et al.*, "Universal power management strategy for triboelectric nanogenerator," *Nano Energy*, vol. 37, pp. 168–176, 2017.

[98] X. Yu, Z. Wang, D. Zhao, J. Ge, T. Cheng, and Z. L. Wang, "Triboelectric nanogenerator with mechanical switch and clamp circuit for low ripple output," *Nano Res.*, vol. 15, pp. 2077–2082, 2022.

[99] D. Bao, L. Luo, Z. Zhang, and T. Ren, "A power management circuit with 50% efficiency and large load capacity for triboelectric nanogenerator," *J. Semicond.*, vol. 38, no. 9, 2017, Art. no. 095001.

[100] A. Kawaguchi, H. Uchiyama, M. Matsunaga, and Y. Ohno, "Simple and highly efficient intermittent operation circuit for triboelectric nanogenerator toward wearable electronic applications," *Appl. Phys. Exp.*, vol. 14, no. 5, 2021, Art. no. 057001.

[101] Z. Wang *et al.*, "Giant performance improvement of triboelectric nanogenerator systems achieved by matched inductor design," *Energy Environ. Sci.*, vol. 14, no. 12, pp. 6627–6637, 2021.

[102] K. Kim, M. Kim, H. Cho, K. Lee, and H.-J. Yoo, "A 55.77 $\mu$W Bio-impedance sensor with 276 $\mu$s settling time for portable blood pressure monitoring system," *J. Semicond. Technol. Sci.*, vol. 17, pp. 912–919, 2017.

[103] L. Corral, A. B. Georgiev, A. Sillitti, and G. Succi, "A method for characterizing energy consumption in android smartphones," in *Proc. 2nd Int. Workshop Green and Sustain. Softw.*, 2013, pp. 38–45.

[104] A. Carroll and G. Heiser, "An analysis of power consumption in a smartphone," in *Proc. USENIX Conf. USENIX Annu. Tech. Conf.*, 2010.

[105] V. Talla, B. Kellogg, S. Gollakota, and J. R. Smith, "Battery-free cellphone," *Proc. ACM Interact., Mobile, Wearable Ubiquitous Technol.*, vol. 1, no. 2, pp. 1–20, 2017.

[106] H. Ryu *et al.*, "High-performance triboelectric nanogenerators based on solid polymer electrolytes with asymmetric pairing of ions," *Adv. Energy Mater.*, vol. 7, no. 17, 2017, Art. no. 1700289.

[107] H.-J. Yoon, H. Ryu, and S.-W. Kim, "Sustainable powering triboelectric nanogenerators: Approaches and the path towards efficient use," *Nano Energy*, vol. 51, pp. 270–285, 2018.

[108] D. O. Bamgboje, W. Harmon, M. Tahan, and T. Hu, "Low cost high performance LED driver based on a self-oscillating boost converter," *IEEE Trans. Power Electron.*, vol. 34, no. 10, pp. 10021–10034, Oct. 2019.

[109] Y. Hu, J. Yang, S. Niu, W. Wu, and Z. L. Wang, "Hybridizing triboelectrification and electromagnetic induction effects for high-efficient mechanical energy harvesting," *ACS Nano*, vol. 8, no. 7, pp. 7442–7450, 2014.

[110] M.-K. Kim, M.-S. Kim, S.-E. Jo, and Y.-J. Kim, "Triboelectric–thermoelectric hybrid nanogenerator for harvesting frictional energy," *Smart Mater. Struct.*, vol. 25, no. 12, 2016, Art. no. 125007.

[111] C. Rodrigues, A. Gomes, A. Ghosh, A. Pereira, and J. Ventura, "Power-generating footwear based on a triboelectric-electromagnetic-piezoelectric hybrid nanogenerator," *Nano Energy*, vol. 62, pp. 660–666, 2019.

[112] Q. Zhang *et al.*, "Electromagnetic shielding hybrid nanogenerator for health monitoring and protection," *Adv. Funct. Mater.*, vol. 28, no. 1, 2018, Art. no. 1703801.

[113] Q. Zhang *et al.*, "Green hybrid power system based on triboelectric nanogenerator for wearable/portable electronics," *Nano Energy*, vol. 55, pp. 151–163, 2019.

[114] J. He *et al.*, "Triboelectric-piezoelectric-electromagnetic hybrid nanogenerator for high-efficient vibration energy harvesting and self-powered wireless monitoring system," *Nano Energy*, vol. 43, pp. 326–339, 2018.

[115] X. Ren *et al.*, "Magnetic force driven noncontact electromagnetic-triboelectric hybrid nanogenerator for scavenging biomechanical energy," *Nano Energy*, vol. 35, pp. 233–241, 2017.
[116] H. Aljarajreh, D. D. Lu, and C. K. Tse, "Synthesis of dual-input single-output DC/DC converters," in *Proc. IEEE Int. Symp. Circuits Syst.*, 2019, pp. 1–5.
[117] B. L. Nguyen, H. Cha, T. Nguyen, and H. Kim, "Family of integrated multi-input multi-output DC-DC power converters," in *Proc. Int. Power Electron. Conf.*, 2018, pp. 3134–3139.
[118] P. Yang, K. T. Chi, J. Xu, and G. Zhou, "Synthesis and analysis of double-input single-output DC/DC converters," *IEEE Trans. Ind. Electron.*, vol. 62, no. 10, pp. 6284–6295, Oct. 2015.

**Tingshu Hu** (Senior Member, IEEE) received the B.S. and M.S. degrees in electrical engineering from Shanghai Jiao Tong University, Shanghai, China, in 1985 and 1988, respectively, and the Ph.D. degree in electrical engineering from the University of Virginia, Charlottesville, VA, USA, in 2001.

She was a Postdoctoral Researcher with the University of Virginia and the University of California, Santa Barbara, USA. In January 2005, she joined the Faculty of Electrical and Computer Engineering, University of Massachusetts Lowell, Lowell, MA, USA, where she is currently a Professor. Her research interests include nonlinear systems theory, optimization, robust control theory, battery modeling and evaluation, control applications in power electronics and power management systems for nanogenerators.

**Haifeng Wang** (Member, IEEE) received the Ph.D. degree in electrical engineering from University of Massachusetts Lowell, Lowell, MA, USA, in 2014.

He is currently an Assistant Professor with Penn State, New Kensington, PA, USA. His research interests include control science, power electronics, computer vision, and deep learning.

Dr. Wang served as the Secretary of IEEE Pittsburgh Section Executive and Administrative Committee.

**William Harmon** received the B.Sc., M.Sc., and Ph.D. degrees in electrical engineering from the Department of Electrical and Computer Engineering, University of Massachusetts Lowell, Lowell, MA, USA, in 2010, 2016, and 2022, respectively.

He has worked professionally in the commercial power electronics industry and currently works as an Electrical Engineer with Raytheon Technologies, Waltham, MA, USA. His research interests include power conversion and power management systems for energy harvesting.

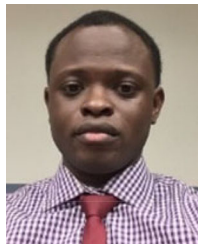

**David Bamgboje** (Member, IEEE) received the B.Sc. degree in electrical engineering from Obafemi Awolowo University, Ile-Ife, Nigeria, in 2012, the M.Sc. degree in electrical engineering from University of Ibadan, Ibadan, Nigeria, in 2016, and the Ph.D. degree in electrical engineering from the University of Massachusetts Lowell, Lowell, MA, USA, in 2019.

His research interests include EMI filters, PFC, high-efficiency power converters, motor control, LED driving systems, and power management systems for nanogenerators.

**Zhong-Lin Wang** received the Ph.D. degree in physics from Arizona State University, Tempe, AZ, USA, in 1987.

He is currently the Director with the Beijing Institute of Nanoenergy and Nanosystems, Chinese Academy of Sciences, Beijing, China, and Regents' Professor and Hightower Chair with Georgia Institute of Technology, Atlanta, GA, USA. He pioneered the nanogenerators field for distributed energy, self-powered sensors and large-scale blue energy. He coined the fields of piezotronics and piezo-phototronics for the third-generation semiconductors. Among 1 00 000 scientists across all fields worldwide, he is ranked #3 in career scientific impact, #1 in Nanoscience, and #2 in Materials Science. His google scholar citation is more than 3 17 000 with an h-index of more than 272.

Dr. Wang has was the recipient of the Celsius Lecture Laureate, Uppsala University, Sweden, in 2020; The Albert Einstein World Award of Science, in 2019; Diels-Planck lecture award, in 2019; ENI award in Energy Frontiers, in 2018; The James C. McGroddy Prize in New Materials from American Physical Society, in 2014; and MRS Medal from Materials Research Society, in 2011. He was elected as a foreign member of the Chinese Academy of Sciences, in 2009, member of European Academy of Sciences, in 2002, Academician of Academia of Sinica, in 2018, International Fellow of Canadian Academy of Engineering, in 2019. He is the Founding Editor and Chief Editor of an international journal *Nano Energy*, which currently has an impact factor of 17.88. Details can be found at: http://www.nanoscience.gatech.edu